Hindawi Publishing Corporation
Journal of Nanomaterials
Volume 2016, Article ID 7314714, 11 pages
http://dx.doi.org/10.1155/2016/7314714

Research Article

Effect of Cadmium Concentration on Structural, Optical, and Electrical Properties of $Cu_2Zn_{1-x}Cd_xSnS_4$ Quinternary Alloy Nanofibres, Synthesized by Electrospinning Technique

A. S. Ibraheam,[1] Y. Al-Douri,[1,2] Nabeel Z. Al-Hazeem,[3] U. Hashim,[1] Deo Prakash,[4] and K. D. Verma[5]

[1]*Institute of Nano Electronic Engineering, Universiti Malaysia Perlis, 01000 Kangar, Perlis, Malaysia*
[2]*Department of Physics, Faculty of Science, University of Sidi-Bel-Abbes, 22000 Sidi-Bel-Abbes, Algeria*
[3]*Nano-Optoelectronics Research and Technology Laboratory, School of Physics, USM, 11800 Penang, Malaysia*
[4]*School of Computer Science & Engineering, Faculty of Engineering, SMVD University, Kakryal, Katra 182320, India*
[5]*Material Science Research Laboratory, Department of Physics, S. V. College, Aligarh 202001, India*

Correspondence should be addressed to Y. Al-Douri; yaldouri@yahoo.com

Received 4 November 2015; Accepted 23 February 2016

Academic Editor: Giovanni Bongiovanni

The $Cu_2Zn_{1-x}Cd_xSnS_4$ quinternary alloy nanofibres with different Cd concentrations were grown on glass substrate using the electrospinning technique. The structural properties of $Cu_2Zn_{1-x}Cd_xSnS_4$ quinternary alloy nanofibres were investigated by X-ray diffraction (XRD), field emission-scanning electron microscopy (FE-SEM), and atomic force microscopy (AFM). Optical properties were analysed through UV-visible spectrophotometry (UV-Vis) and photoluminescence (PL) spectroscopy, which revealed that there is a decrease in band gap from 1.75 eV to 1.61 eV, with the increasing Cd concentration from $x = 0$ to $x = 1$. The current-voltage measurements exhibited a power conversion efficiency of 3% under the solar illumination with intensity of 100 mW/cm^2. Electrical properties supported that the $Cu_2Zn_{1-x}Cd_xSnS_4$ quinternary alloy can be used as an absorber in solar cells. The bulk modulus, refractive index, and dielectric constant were also investigated.

1. Introduction

The quaternary $CuIn_{1-x}Ga_xSe_2$ (CIGS) thin film is a promising candidate for low cost absorber layer in thin film solar cell, due to its excellent properties and higher efficiency [1–3]. In recent years, enormous efforts have been dedicated to find out the low cost, earth-abundant elements materials for solar cell applications. Cu_2ZnSnS_4 (CZTS) is a potential material to substitute the $CuIn_{1-x}Ga_xSe_2$ (CIGS) and has attracted great interest due to its direct band gap of $E_g = 1.45$–1.5 eV, optical absorption coefficient higher than 10^4 cm^{-1} [4], good photostability [5], low toxicity [6], high photovoltaic efficiency [7], and presence of earth-abundant elements [8–13]. Various technologies have been developed for deposition of CZTS, which include thermal evaporation [14–16], sputtering [17], electrodeposition [18, 19], spray pyrolysis [20], electrochemical deposition [21], and pulsed laser deposition [22–24]. Third-generation approaches to photovoltaics (PVs) aim to decrease costs and significantly increasing efficiencies but maintain the economic and environmental cost advantages of thin-film deposition techniques. PV technologies have shown significant progress lately in terms of annual production capacity and life cycle environmental performances, which necessitates the assessment of environmental impacts of such technologies. The different PV technologies show slight variations in the emissions when comparing the emissions from conventional energy technologies replaced by the latest PV technologies.

Lately, Spinelli et al. [25] have proposed dielectric nanoparticle arrays as antireflection coatings and light-trapping schemes for thin-film c-Si solar cells. However, practical aspects about the integration of these nanostructures with solar modules have yet to be investigated. They have studied the effect of ethylene vinyl acetate (EVA) encapsulation on the

optical properties of dielectric nanoparticles placed on top of c-Si substrates and showed that Si nanoparticle encapsulated in EVA layer yields ultralow reflectivity over the entire 300–1000 nm spectral range. Furthermore, they have studied the case of plasmonic nanoparticle coatings for c-Si solar cells. Breitenstein [26] has investigated novel one-diode model for illuminated solar cells, which contains an additional variable resistance describing minority carrier diffusion from the bulk to the p-n junction. This model naturally describes the differences between photo- and electroluminescence imaging, as well as a well-known departure from the superposition principle. Oishi et al. [27] have grown Cu_2ZnSnS_4 thin films on Si (100) substrate by vacuum evaporation technique, which exhibited the broad emissions at around 1.45 eV and 1.31 eV in the photoluminescence spectrum measured at 13 K.

Electrospinning technique is one of the most promising methods for the fabrication of 1D-nanostructure materials [28]. Researches on the synthesis of various metal-oxide nanowires, via electrospinning, have recently increased [29, 30]. The electrospinning route is a simple, versatile, and relatively inexpensive technique for the synthesis of a broad range of hybrid nanocomposites. Unlike other methods, it can produce short nanorods or nanotubes, along with the continuous nanowires and nanotubes [31]. For the first time, electrospinning technique was successfully used for the synthesis of CZTS fibres [32].

In this work, electrospinning technique has been described as an alternative synthesis route for the preparation of $Cu_2Zn_{1-x}Cd_xSnS_4$ quinternary alloy nanofibres, which were further studied as the photovoltaic (PV) absorber layers without sulfurization. The obtained $Cu_2Zn_{1-x}Cd_xSnS_4$ quinternary alloy nanofibres were analysed and characterized, and the optimum Cd concentration (x) for PVs applications was determined. In addition, the bulk modulus, refractive index, and optical dielectric constant were also investigated.

2. Experimental Process

$Cu_2Zn_{1-x}Cd_xSnS_4$ quinternary alloy nanofibres were deposited onto glass substrate using the electrospinning method. Firstly, the precursor solutions were prepared from copper (II) chloride dihydrate, zinc (II) chloride dihydrate, tin (II) chloride dihydrate, cadmium (II) chloride, thiourea, 2-methoxyethanol (2-metho), and monoethanolamine (MEA). The molar ratio of Cu, (Zn + Cd), Sn, and S in the solution was 2 : 1 : 1 : 4. To obtain the solutions with different Cd concentration (x), the molar ratio of Cd to (Zn + Cd) was varied to give x values of 0, 0.2, 0.4, 0.6, 0.8, and 1. The precursor solutions were mixed on the basis of required ratio of the formula, that is, $Cu_2{}^{+2}(Zn_{1-x}Cd_x)^{+2}Sn^{+4}S_4{}^{-8}$. The 2-metho and MEA were used as solvent and stabilizer, respectively. The molar ratio of MEA to precursor solution of $Cu_2Zn_{1-x}Cd_xSnS_4$ was maintained at 0.5. The solution was stirred at 50°C for 3 h to completely dissolve the metal salts, followed by addition of thiourea, which results in the yellow and transparent solution. After that, polyvinyl alcohol (PVA) was weighted precisely (concentration ratios of 25 wt.%) and mixed with solution of $Cu_2Zn_{1-x}Cd_xSnS_4$ (x = 0, 0.2, 0.4, 0.6, 0.8, 1), under vigorous magnetic stirring for 20 h, leading to a clear white solution. During a typical electrospinning process, 2 mL of the above solution was added into the syringe which was pumped with a flow rate of 0.6 mL/h, at a voltage of 12 kV and the electrode distance of 12 cm. Precursor fibres collected on glass substrate were then annealed at 300°C under N_2 atmosphere for 40 min.

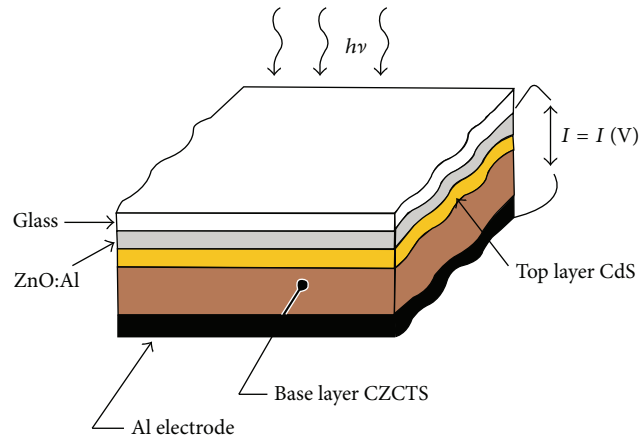

Figure 1: Schematic structure of typical $Cu_2Zn_{0.4}Cd_{0.6}SnS_4$ solar cell.

To study the performance of solar cells based on $Cu_2Zn_{0.4}Cd_{0.6}SnS_4$ quinternary alloy nanofibres, prototype of CZCTS solar cells with Cd concentration equals 0.6 was prepared. The CdS and ZnO:Al were successively deposited on $Cu_2Zn_{0.4}Cd_{0.6}SnS_4$ quinternary alloy to obtain ZnO:Al/CdS/$Cu_2Zn_{0.4}Cd_{0.6}SnS_4$/Al/glass structure, including Al doped ZnO which equals 5% as shown in Figure 1.

The crystal structure of the $Cu_2Zn_{1-x}Cd_xSnS_4$ quinternary alloy nanofibres was examined by X-ray diffraction (XRD; PW 1710 X-ray diffractometer, Phillips, USA) with Cu Kα radiation (λ = 1.54 Å). The optical properties were measured at room temperature using UV-visible spectrophotometry (UV-vis; Lambda 950, PerkinElmer, USA) and photoluminescence spectroscopy (PL; Jobin Yvon model HR 800 UV system, Jobin Yvon, USA) was carried out at room temperature using a He-Cd laser (λ = 325 nm). Surface morphology and grain size were investigated by field emission-scanning electron microscopy (FE-SEM; NOVA NANO SEM 450, USA). The topography of the films was characterized by atomic force microscopy (AFM; SII SPI 3800N Probe, Seiko Instruments Inc., USA). For the power conversion efficiency measurement of $Cu_2Zn_{0.4}Cd_{0.6}SnS_4$ based solar cell, the current-voltage characteristics were measured under simulated AM 1.5 G solar illumination with intensity of 100 mW/cm^2.

3. Results and Discussion

3.1. Structural Properties. Figure 2 shows the XRD patterns of CZCTS quinternary alloy nanofibres obtained from 15 wt.% PVA/CZTS nanofibres at x = 0 and the increasing concentration ratios of 25 wt.% (PVA) at x = 0.2, 0.4, 0.6, 0.8, and 1. The XRD patterns of $Cu_2Zn_{1-x}Cd_xSnS_4$ quinternary alloy nanofibres show five peaks at 2θ = 16.147°, 28.436°, 32.986°, 34.549°, and 47.875° that attributed to (002), (112),

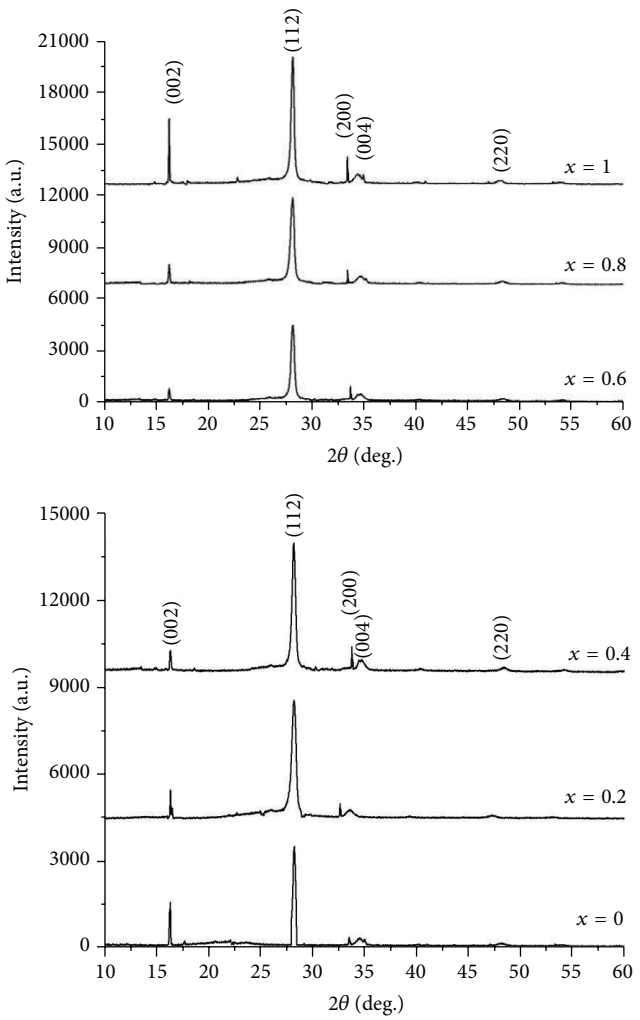

FIGURE 2: XRD patterns of $Cu_2Zn_{1-x}Cd_xSnS_4$ quinternary alloy nanofibres at different Cd concentrations ($x = 0$–1).

(200), (004), and (220) planes of the tetragonal kesterite phase of Cu_2ZnSnS_4 (ICDD PDF2008, 01-075-4122) and stannite phase of Cu_2CdSnS_4 (ICDD (PDF2008), 00-029-0537). The estimated errors as given in Table 1 are accomplished based on three prepared samples for each concentration. As seen, the peak intensity of (112) was higher than (002) and (200), revealing that (112) is the preferred growth plane, which is comparable to the standard XRD pattern of CZTS [33]. The peaks were shifted to the lower angle side with increasing Cd concentration in the $Cu_2Zn_{1-x}Cd_xSnS_4$ quinternary alloy nanofibres, due to the increasing lattice constant. This is due to radius of Cd ion (1.53 Å), which is larger than Zn (1.33 Å), as supported by previous work [34]. It is important to note that XRD patterns of $Cu_2Zn_{1-x}Cd_xSnS_4$ nanofibres showed no additional peaks corresponding to other impurities, such as CdS, ZnS, CuS, or Cu_2S, over the entire composition range. The lattice constants a and c were calculated for the CZTS nanocrystals based on the (112) peak, which are given in Table 1:

$$\left(\frac{1}{d^2}\right) = \frac{\left(h^2 + k^2\right)}{a^2} + \left(\frac{l^2}{c^2}\right). \quad (1)$$

The crystallite sizes (D) of CZCTS nanofibre were calculated using the Scherrer formula for the peak (112) [35]:

$$D = \frac{k\lambda}{\beta \cos\theta}, \quad (2)$$

where k is a constant, taken to be 0.94, and β is the full width at half maximum (FWHM).

Material stiffness is important in different industries, which is reflected in bulk modulus [36–41]. Many attempts have been made to explore the thermodynamic properties of solids. In the present study, thermodynamic properties, including interatomic separation and bulk modulus of solids, have been studied with different approximations and best-fit relations [38–42]. Additionally, more approaches that are empirical have been developed to accurately compute the structural and electronic properties of the solids, despite *ab initio* calculations, which are very complex and require numerous efforts [43]. Although the empirical methods give applicability advantage to a broad class of materials and illustrate the trends in many cases, they might not be extremely accurate for each specific material.

Cohen [44] had established an empirical formula for the calculation of bulk modulus B_0. This formula was based on the nearest-neighbour distance and presented good consistency of results with the experimental data. At the same time, an analytical expression for the calculation of bulk modulus from the total energy has been derived by Lam et al. [45], which was structurally different from the empirical formula and yet offered the same numerical results. In addition, they have obtained an analytical expression of the bulk modulus. Another concept based on lattice constant has been established [46], where the obtained results are consistent with the experimental data and other calculations. The two interesting features of this formula are as follows: only the lattice constant is required as input and the computation of B_0 is trivial.

To determine the possible relation of bulk modulus with the lattice constant (despite being a qualitative concept) is the main objective. It was advocated that the dominant effect is the degree of covalence, which was characterized by the Phillips homopolar gap E_h [42]. The reason to include these data in present work is the validity of calculations which is not restricted in computed space. Thus, it will not be wrong to consider that the data might be proven valuable for the future work in this field. Here the study of B_0 is important, as the differences between the lattice constants of $Cu_2Zn_{1-x}Cd_xSnS_4$ quinternary alloy nanofibres can be clearly seen in Table 1. Here, B_0 was calculated using the following empirical formula [46]:

$$B_0 = [3000 - 100\lambda]\left(\frac{a}{2}\right)^{-3.5}, \quad (3)$$

where a is the lattice constant (in Å); λ is an empirical parameter for the effect of ionicity ($\lambda = 0$, 1, 2 for groups IV, III–V, and II–VI semiconductors, resp.). The calculated values of B_0 are indicated in Table 1. Here it can be concluded that the present bulk modulus, calculated in a different way from the definition of Cohen, exhibit the same trends. It was

Table 1: The structural properties of $Cu_2Zn_{1-x}Cd_xSnS_4$ quinternary alloy nanofibres using XRD for different Cd concentrations, $x = 0$–1.

x	Peak (θ)	Crystallite size (nm)	d_{hkl} (112) (Å)	Lattice constants (Å)	Bulk modulus (B_0) (GPa)	Estimated error (%)
0	28.436	30.90	3.387	$a = 5.339$ $a = 5.428^*$ $c = 10.507$ $c = 10.842^*$	82.30	1
0.2	28.428	39.79	3.545	$a = 5.434$ $c = 10.808$	84.20	1.5
0.4	28.398	49.66	3.623	$a = 5.438$ $c = 10.820$	84.25	1.5
0.6	28.388	56.34	3.695	$a = 5.583$ $c = 10.831$	85.15	1.5
0.8	28.383	59.86	3.734	$a = 5.567$ $c = 11.168$	85.05	1.5
1	28.379	64.28	3.804	$a = 5.668$ $a = 5.487^\#$ $c = 11.349$ $c = 11.389^*$	87.07	1

*Ref. [34, 47] exp., #ref. [47] exp.

observed that Cd concentration was directly proportional to the stiffness of $Cu_2Zn_{1-x}Cd_xSnS_4$ quinternary alloy nanofibres.

3.2. Morphological Study. The morphology of the $Cu_2Zn_{1-x}Cd_xSnS_4$ quinternary alloy nanofibres was studied using FE-SEM. Figure 3 shows a series of FE-SEM images of PVA/$Cu_2Zn_{1-x}Cd_xSnS_4$ quinternary alloy nanofibres obtained from precursor solutions, with concentration ratios of 15 and 25 wt.% (PVA) and different x values ($x = 0$, 0.2, 0.4, 0.6, 0.8, and 1). The formation of fibres can be easily controlled by optimizing the PVA concentration. At low concentration, formation of defects such as beads along the fibres was observed (Figure 3 ($x = 0$)), which is due to the capillary breakup of the spinning jet because of surface tension [47]. Also, increasing the concentration of polymer (PVA) in solution with increasing Cd concentration, the number of defects was found to decrease, resulting in the formation of uniform fibres with increasing diameters from 58.615 for $x = 0$, 125.582 for $x = 0.2$, 134.21 for $x = 0.4$, 185.33 for $x = 0.6$, 290.45 for $x = 0.8$, and 424.85 for $x = 1$. This suppression of defects during the fibre formation can perhaps be understood as follows: increasing concentration of solution helps to raise the viscoelastic forces, which might have resulted in reducing the influential forces due to surface tension. The obtained results illustrate that the morphology of the composite fibres was optimized with minimal defects when the PVA concentration was 25 wt.% ($x = 1$). It can be seen from the FE-SEM images that a random mesh of nanofibres was obtained. This randomness of the fibre mesh was the direct consequence of bending instability associated with the electrospinning jet.

AFM was used to confirm the cylindrical morphology of the electrospinned fibres. Figure 4 displays the AFM images of PVA/$Cu_2Zn_{1-x}Cd_xSnS_4$ nanofibres obtained from precursor solutions with 15 wt.% of PVA at $x = 0$ and 25 wt.% of PVA at $x = 0.2$, 0.4, 0.6, 0.8, and 1. From Figure 4, it is obvious that the PVA/$Cu_2Zn_{1-x}Cd_xSnS_4$ has the cylindrical morphology. The fibres were uniformly distributed over the collector screen. The average roughness of the surface was observed to be 25.6, 46.3, 96.6, 124, 188.50, and 236.23 nm at $x = 0$, 0.2, 0.4, 0.6, 0.8, and 1, respectively. These results indicate that the quality of $Cu_2Zn_{1-x}Cd_xSnS_4$ quinternary alloy nanostructure is improved as the Cd concentration increases.

3.3. Optical Properties. PL spectra of CZCTS quinternary alloy nanofibres with different Cd concentrations measured at room temperature are shown in Figure 5. PL spectra consist of one broad asymmetric band at 1.75 eV for Cu_2ZnSnS_4 and at 1.61 eV for Cu_2CdSnS_4 as given in Table 2. A shift of the PL band of $Cu_2Zn_{1-x}Cd_xSnS_4$ quinternary alloy nanofibres towards higher wavelengths with increasing Cd concentration was observed in the region $0 \leq x \leq 1$. This shifting is due to the substitution of Zn atoms with Cd atoms to produce a lower energy gap [48, 49].

The absorption coefficient associated with the high absorption region was calculated from absorbance (A) and the film thickness (t) using the following relation:

$$a = 2.303\frac{A}{t}. \quad (4)$$

Figure 6 shows the absorption coefficient (α) of $Cu_2Zn_{1-x}Cd_xSnS_4$ quinternary alloy nanofibres deposited at different Cd concentration ($x = 0$ to 1). It can be observed that the absorption coefficient was greater than 10^4 cm^{-1}. Thus, it would be better to infer that the grown nanostructures have good absorbance in the visible region of electromagnetic spectrum. The absorption spectra are shifted towards longer wavelengths as Cd concentration increases. The fundamental

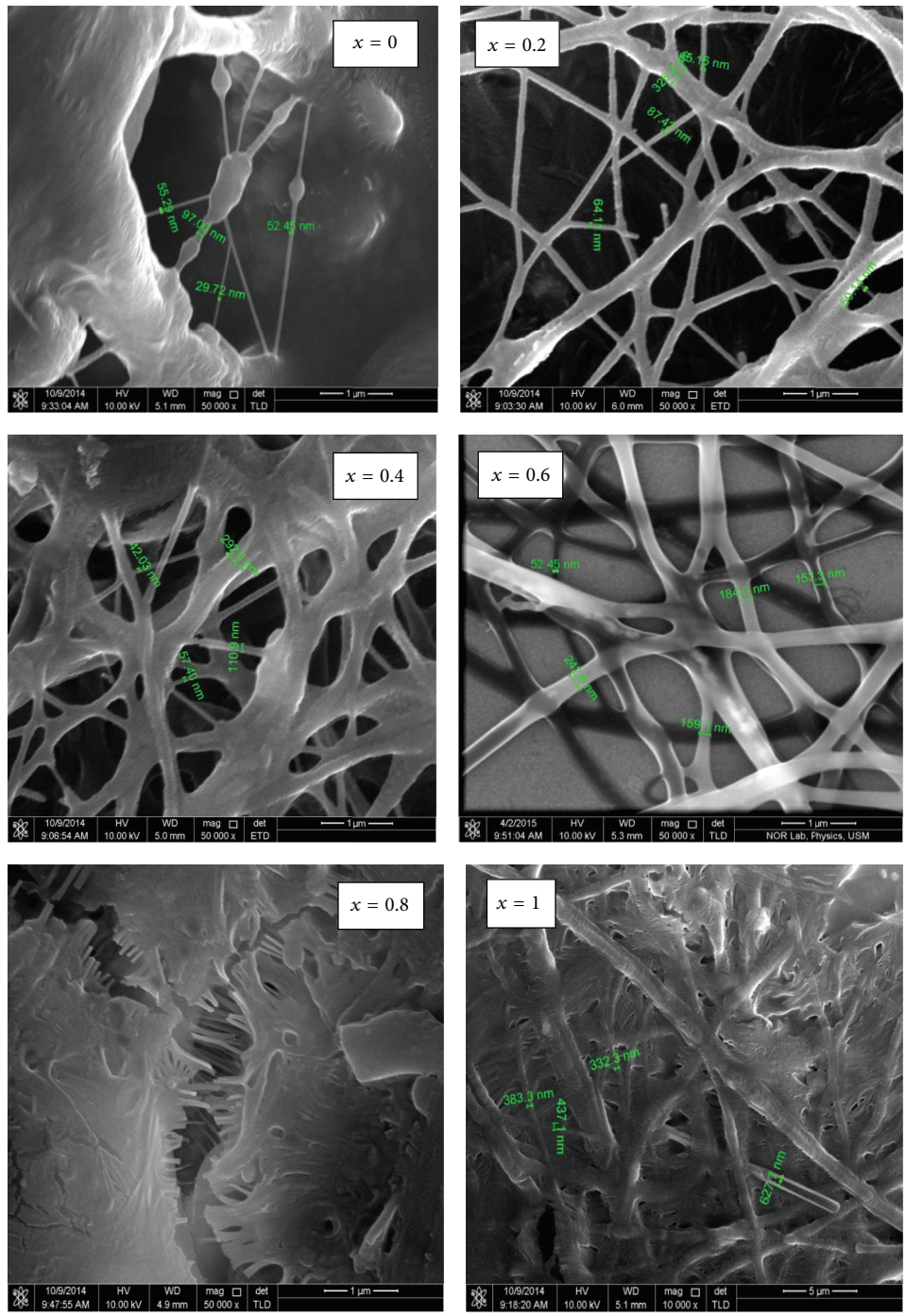

Figure 3: FE-SEM images of $Cu_2Zn_{1-x}Cd_xSnS_4$ quinternary alloy nanofibre at different Cd concentrations ($x = 0$–1).

absorption corresponds to the transition from valence to conduction band that can be used to determine the band gap of the material. The energy band gap (E_g) was estimated using

$$(h\nu\alpha)^{\gamma} = \beta\left(h\nu - E_g\right), \tag{5}$$

where $h\nu$ is the incident photon energy, β is parameter, and γ is index which characterizes the optical absorption process ($\gamma = 2$ and 1/2 for indirect and direct transitions, resp.). The best linear fit was obtained for $\gamma = 1/2$ for direct transition. E_g was determined by extrapolating the straight line portion $(h\nu\alpha)^{\gamma} = 0$ value and showed a decrease from 1.81 eV for $x = 0$ to 1.80 eV for $x = 0.2$, 1.79 eV for $x = 0.4$, 1.69 eV for $x = 0.6$, 1.68 for $x = 0.8$, and 1.63 for $x = 1$, as illustrated in Figure 7 and given in Table 2. It was found that the energy band gap of $Cu_2Zn_{1-x}Cd_xSnS_4$ quinternary alloy nanofibres drifts towards lower energy with an increase in Cd concentration.

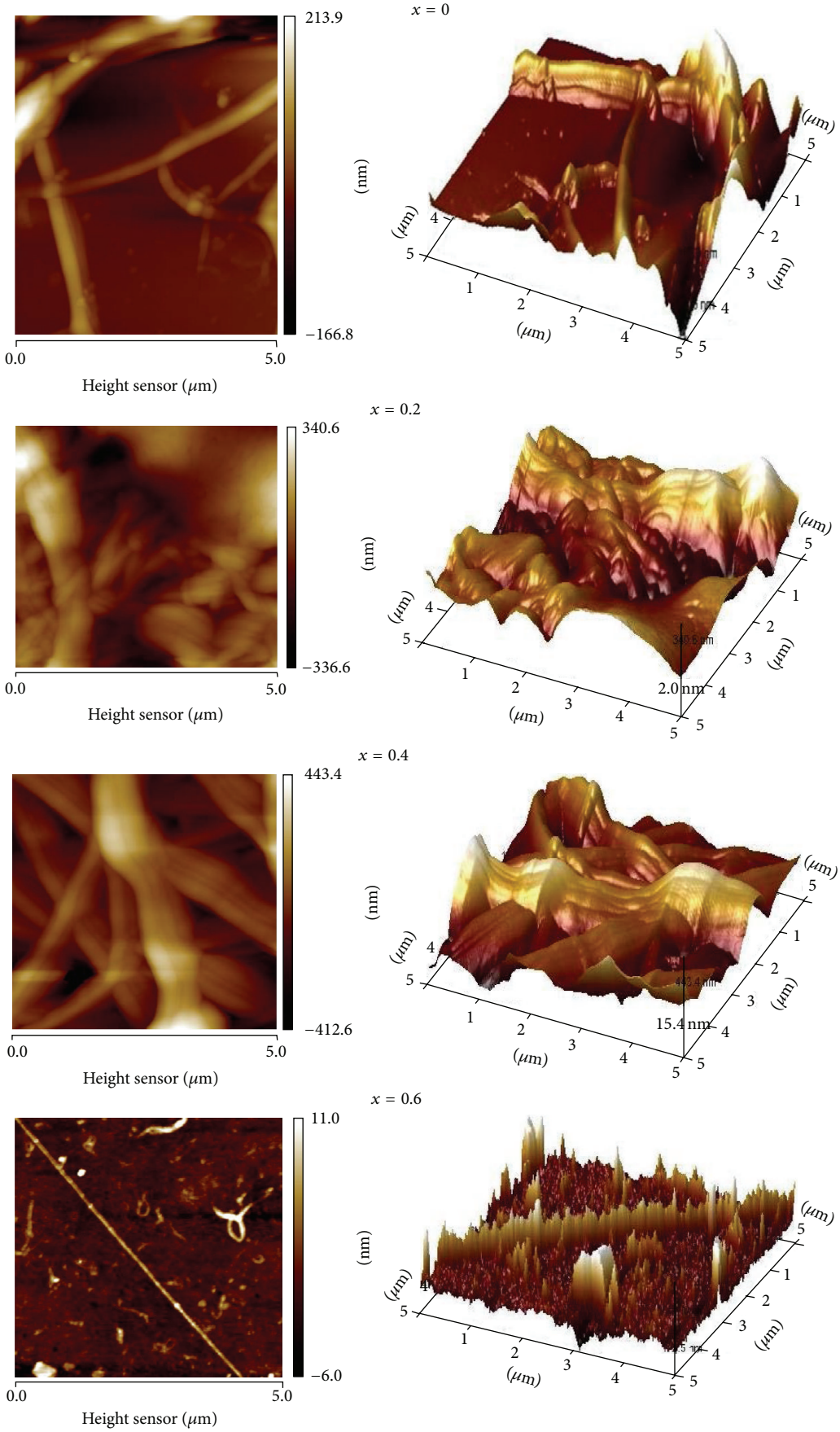

Figure 4: Continued.

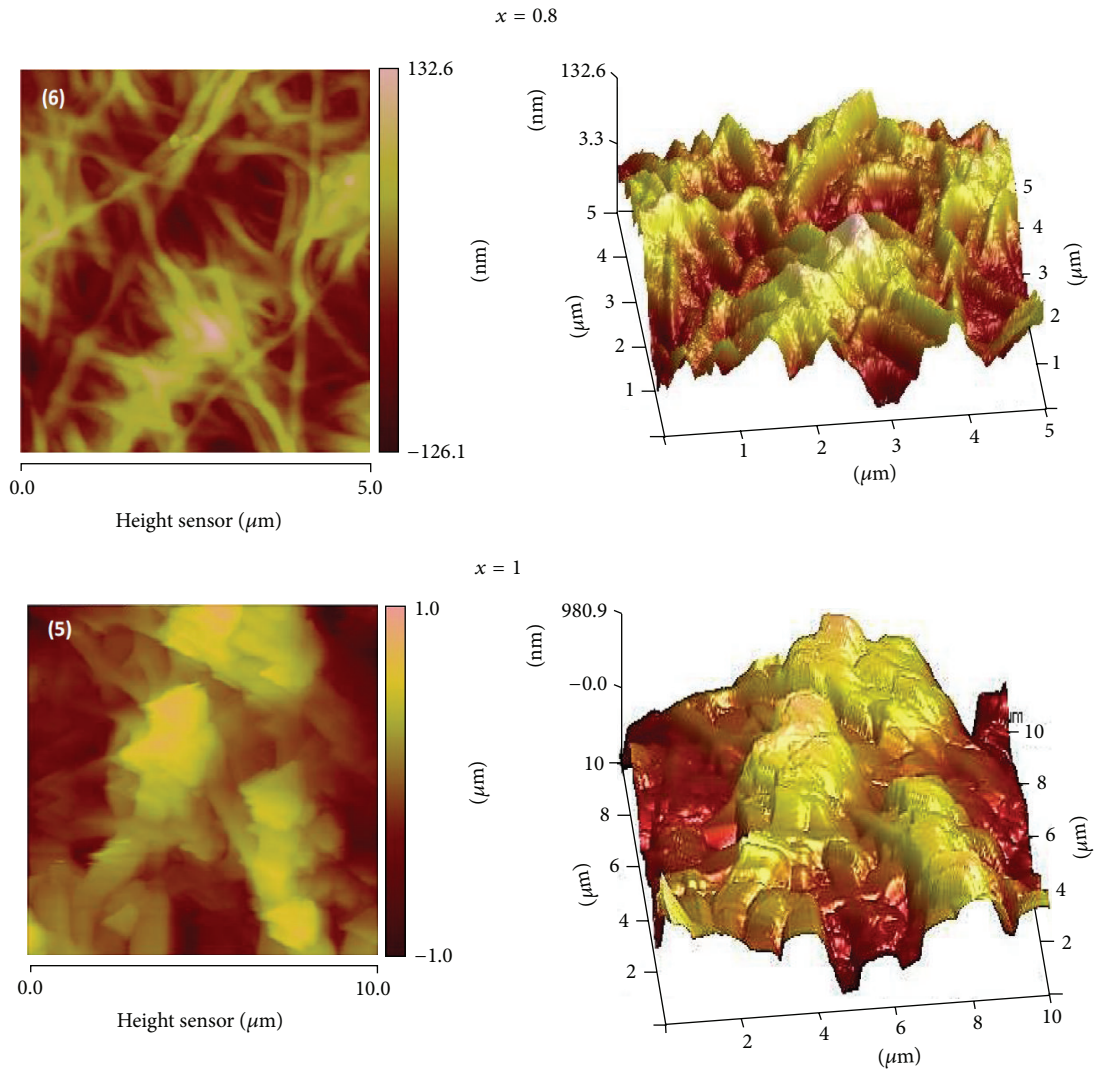

FIGURE 4: AFM images of $Cu_2Zn_{1-x}Cd_xSnS_4$ quinternary alloy nanofibres at different Cd concentrations ($x = 0$–1).

Thus, the optical properties of CZCTS absorber layers can be improved by substituting the Zn atoms by Cd atoms to produce a lower energy gap [34].

The refractive index n is a significant physical parameter in microscopic atomic interactions. Theoretically, the refractive index is related to the density and the local polarizability of these entities [50]. Many simple relationships between refractive index n and the energy gap E_g have been attempted [51–58]. Here, various relationships between n and E_g have been reviewed in order to validate the current work. As suggested by Ravindra et al. [51], the band gap and the high frequency refractive index presented a linear relationship:

$$n = \alpha + \beta E_g, \tag{6}$$

where $\alpha = 4.048$ and $\beta = -0.62\ \text{eV}^{-1}$

Inspired by simple physics of light refraction and dispersion, Hervé and Vandamme [52] have proposed an empirical relation as

$$n = \sqrt{1 + \left(\frac{A}{E_g + B}\right)^2}, \tag{7}$$

where $A = 13.6$ eV and $B = 3.4$ eV.

Ghosh et al. [53] had taken a different approach by considering the band structural and quantum-dielectric formulations of Penn [59] and Van Vechten [60]. Introducing A (contribution from the valence electrons) and B (constant additive to the lowest band gap E_g), the expression was written as

$$n^2 - 1 = \frac{A}{\left(E_g + B\right)^2}, \tag{8}$$

where $A = 25E_g + 212$, $B = 0.21E_g + 4.25$, and $(E_g + B)$ refers to an appropriate average energy gap of the material.

Thus, these three models for variation of n with energy gap have been tried. In addition, the calculated values of

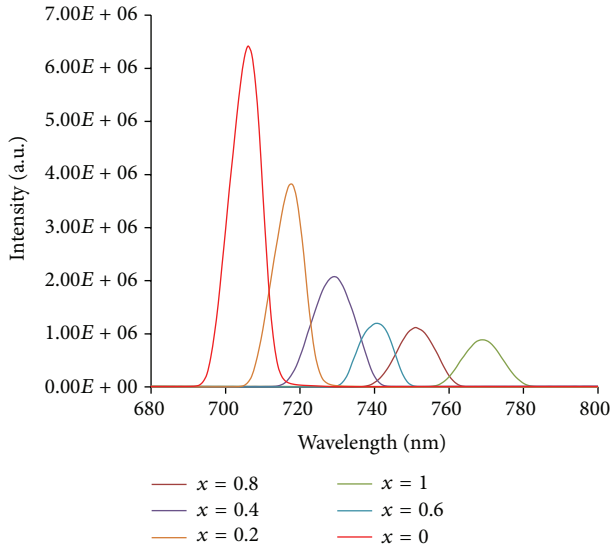

FIGURE 5: PL of $Cu_2Zn_{1-x}Cd_xSnS_4$ quinternary alloy nanofibres at different Cd concentrations ($x = 0$–1).

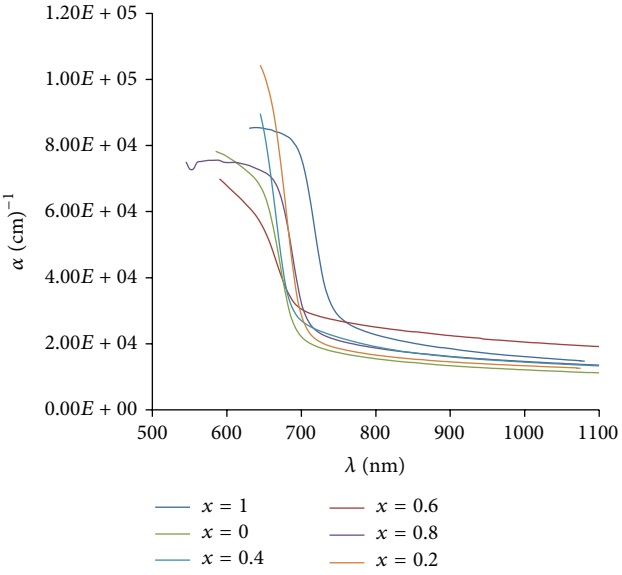

FIGURE 6: Absorption coefficient of $Cu_2Zn_{1-x}Cd_xSnS_4$ quinternary alloy nanofibres at different Cd concentrations ($x = 0$–1).

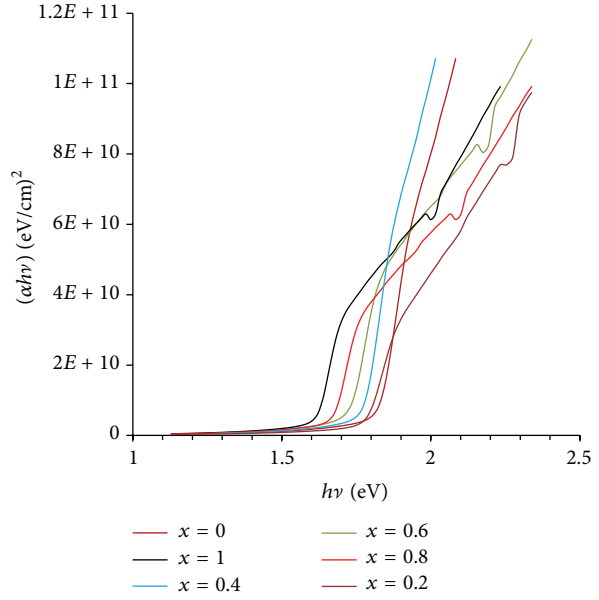

FIGURE 7: Optical band gap of $Cu_2Zn_{1-x}Cd_xSnS_4$ quinternary alloy nanofibres at different Cd concentrations ($x = 0$–1).

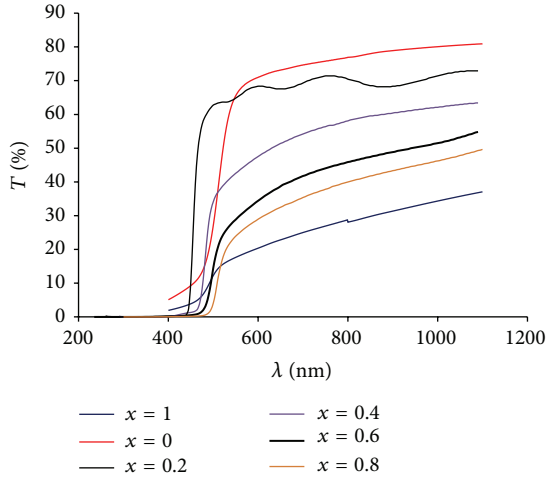

FIGURE 8: Transmittance spectra of $Cu_2Zn_{1-x}Cd_xSnS_4$ quinternary alloy nanofibres at different Cd concentrations ($x = 0$–1).

the optical dielectric constant (ε_∞) were obtained using the relation $\varepsilon_\infty = n^2$ [61]. The calculated refractive index and optical dielectric constant are given in Table 2. This is showing that the Ghosh et al. model is an appropriate model for solar cells applications.

Figure 8 shows the transmittance spectra of the $Cu_2Zn_{1-x}Cd_xSnS_4$ quinternary alloy nanofibres at different Cd concentrations. The transmittance of the nanofibres decreases as Cd concentration increases, which is attributed to the increasing absorbance. The highest value of transmittance was 78% at $x = 0$ and the lowest was 33% at $x = 1$, with a shift in transmittance towards high wavelengths as Cd concentration increases.

3.4. I-V Characteristics. To study the performance of CZCTS-based solar cells, the optimal prototype device with glass/ZnO:Al/CdS/$Cu_2Zn_{0.8}Cd_{0.2}SnS_4$/Al structure was prepared (Figure 1). *I-V* curve was studied under 100 mW/cm^2 via simulated AM 1.5 G solar illuminations (Figure 9). Our results suggest that $Cu_2Zn_{1-x}Cd_xSnS_4$ at x equals 0.6, has an optimal band gap, and can be a suitable material as absorber layer in single junction solar cells. Although the power conversion efficiency (3%) is low without elaborate optimization (Figure 9), our preliminary results suggest that the performance of CZCTS-based solar cells is quite tunable

Table 2: The energy band gaps corresponding to refractive index and optical dielectric constant using Ravindra et al. [51], Hervé and Vandamme [52], and Ghosh et al. [53] of $Cu_2Zn_{1-x}Cd_xSnS_4$ quinternary alloy nanofibres.

x	Band gap using UV (eV)*	Band gap using PL (eV)**	n	ε_{∞}
0	1.81	1.75	2.95^{a*} 2.82^{b*} 2.70^{c*} 2.83^{a**} 2.70^{b**} 2.58^{c**}	8.70^{a*} 7.95^{b*} 7.29^{c*} 8.00^{a**} 7.29^{b**} 6.65^{c**}
0.2	1.80	1.72	2.97^{a*} 2.84^{b*} 2.72^{c*} 2.85^{a**} 2.73^{b**} 2.61^{c**}	8.82^{a*} 8.06^{b*} 7.39^{c*} 8.12^{a**} 7.45^{b**} 6.81^{c**}
0.4	1.79	1.70	2.99^{a*} 2.86^{b*} 2.74^{c*} 2.87^{a**} 2.75^{b**} 2.63^{c**}	8.94^{a*} 8.17^{b*} 7.50^{c*} 8.23^{a**} 7.56^{b**} 6.91^{c**}
0.6	1.69	1.67	3.01^{a*} 2.88^{b*} 2.76^{c*} 2.89^{a**} 2.77^{b**} 2.65^{c**}	9.06^{a*} 8.29^{b*} 7.61^{c*} 8.35^{a**} 7.67^{b**} 7.02^{c**}
0.8	1.68	1.65	3.04^{a*} 3.00^{b*} 2.78^{c*} 2.91^{a**} 2.79^{b**} 2.68^{c**}	9.24^{a*} 9.00^{b*} 7.72^{c*} 8.46^{a**} 7.78^{b**} 7.18^{c**}
1	1.63	1.61	3.07^{a*} 3.02^{b*} 2.81^{c*} 2.93^{a**} 2.82^{b**} 2.71^{c**}	9.42^{a*} 9.12^{b*} 7.89^{c*} 8.58^{a**} 7.95^{b**} 7.34^{c**}

[a]Ref. [51]; [b]ref. [52]; [c]ref. [53].
*refers to Band gap using UV.
**refers to Band gap using PL.

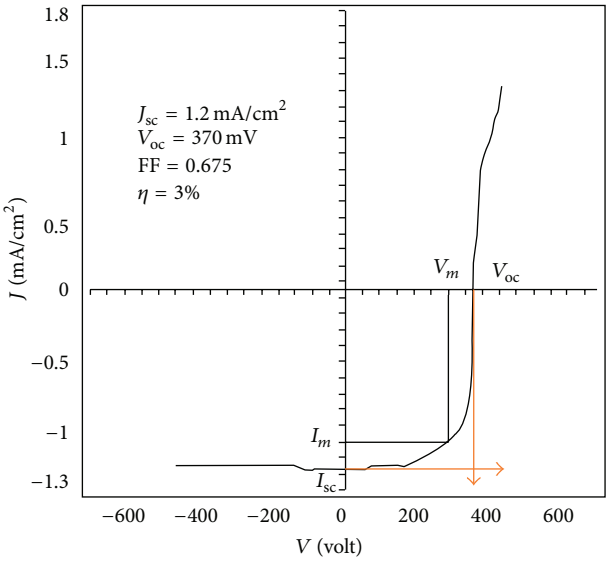

Figure 9: I-V characteristics for the glass/ZnO:Al/CdS/$Cu_2Zn_{0.4}Cd_{0.6}SnS_4$/Al solar cell at Cd concentration $x = 0.6$.

at varied Cd concentration [34]. It is of prime importance to consider the trade-off between various parameters and the design of tandem solar cells with the optimal performance.

4. Conclusion

In this work, $Cu_2Zn_{1-x}Cd_xSnS_4$ quinternary alloys nanofibres were successfully fabricated via electrospinning technique. Our findings suggest that the Cd concentrations correlate directly with the lattice constant and bulk modulus that reflect the stiffness of $Cu_2Zn_{1-x}Cd_xSnS_4$ quinternary alloys nanofibres. The diameters of nanofibres were found to be in between 58.615 and 442.85 nm at $x = 0$ and 1, respectively. The band gap is found to decrease with increasing Cd concentrations. The power conversion efficiency of the $Cu_2Zn_{1-x}Cd_xSnS_4$-based solar cells with Cd concentration, $x = 0.6$, is 3%. Ghosh et al. model is found to be more appropriate for solar cells application.

Competing Interests

The authors declare that they have no competing interests.

Acknowledgments

Y. Al-Douri would like to thank Universiti Malaysia Perlis for Grant no. 9007-00185. K. D. Verma would like to acknowledge U.G.C., New Delhi, India, for providing financial assistance in the form of Major Research Project (code: 42-856/2013(SR)).

References

[1] C. Steinhagen, M. G. Panthani, V. Akhavan, B. Goodfellow, B. Koo, and B. A. Korgel, "Synthesis of Cu_2ZnSnS_4 nanocrystals for use in low-cost photovoltaics," *Journal of the American Chemical Society*, vol. 131, no. 35, pp. 12554–12555, 2009.

[2] Q. Guo, H. W. Hillhouse, and R. Agrawal, "Synthesis of Cu_2ZnSnS_4 nanocrystal ink and its use for solar cells," *Journal of the American Chemical Society*, vol. 131, no. 33, pp. 11672–11673, 2009.

[3] S. C. Riha, B. A. Parkinson, and A. L. Prieto, "Solution-based synthesis and characterization of Cu_2ZnSnS_4 nanocrystals," *Journal of the American Chemical Society*, vol. 131, no. 34, pp. 12054–12055, 2009.

[4] B. Shin, O. Gunawan, Y. Zhu, N. A. Bojarczuk, S. J. Chey, and S. Guha, "Thin film solar cell with 8.4% power conversion efficiency using an earth-abundant Cu_2ZnSnS_4 absorber," *Progress in Photovoltaics: Research and Applications*, vol. 21, no. 1, pp. 72–76, 2013.

[5] C. Tablero, "Electronic and photon absorber properties of Cr-doped Cu_2ZnSnS_4," *Journal of Physical Chemistry C*, vol. 116, no. 44, pp. 23224–23230, 2012.

[6] A. Walsh, S. Chen, S.-H. Wei, and X.-G. Gong, "Kesterite thin-film solar cells: advances in materials modelling of Cu_2ZnSnS_4," *Advanced Energy Materials*, vol. 2, no. 4, pp. 400–409, 2012.

[7] T. Todorov and D. B. Mitzi, "Direct liquid coating of chalcopyrite light-absorbing layers for photovoltaic devices," *European Journal of Inorganic Chemistry*, vol. 2010, no. 1, pp. 17–28, 2010.

[8] J.-S. Seol, S.-Y. Lee, J.-C. Lee, H.-D. Nam, and K.-H. Kim, "Electrical and optical properties of Cu_2ZnSnS_4 thin films prepared by rf magnetron sputtering process," *Solar Energy Materials and Solar Cells*, vol. 75, no. 1-2, pp. 155–162, 2003.

[9] K. Tanaka, Y. Fukui, N. Moritake, and H. Uchiki, "Chemical composition dependence of morphological and optical properties of Cu_2ZnSnS_4 thin films deposited by sol-gel sulfurization and Cu_2ZnSnS_4 thin film solar cell efficiency," *Solar Energy Materials and Solar Cells*, vol. 95, no. 3, pp. 838–842, 2011.

[10] L. Sun, J. He, H. Kong, F. Yue, P. Yang, and J. Chu, "Structure, composition and optical properties of Cu_2ZnSnS_4 thin films deposited by Pulsed Laser Deposition method," *Solar Energy Materials and Solar Cells*, vol. 95, no. 10, pp. 2907–2913, 2011.

[11] S. Schorr, "The crystal structure of kesterite type compounds: a neutron and X-ray diffraction study," *Solar Energy Materials and Solar Cells*, vol. 95, no. 6, pp. 1482–1488, 2011.

[12] T. Rath, W. Haas, A. Pein et al., "Synthesis and characterization of copper zinc tin chalcogenide nanoparticles: influence of reactants on the chemical composition," *Solar Energy Materials and Solar Cells*, vol. 101, pp. 87–94, 2012.

[13] C.-R. Li, Y.-F. Li, B. Yao et al., "Electronic and optical properties of kesterite Cu_2ZnSnS_4 under in-plane biaxial strains: first-principles calculations," *Physics Letters A*, vol. 377, no. 37, pp. 2398–2402, 2013.

[14] B. Shin, O. Gunawan, Y. Zhu, N. A. Bojarczuk, S. J. Chey, and S. Guha, "Thin film solar cell with 8.4% power conversion efficiency using an earth-abundant Cu_2ZnSnS_4 absorber," *Progress in Photovoltaics: Research and Applications*, vol. 21, no. 1, pp. 72–76, 2011.

[15] A. Weber, H. Krauth, S. Perlt et al., "Multi-stage evaporation of Cu_2ZnSnS_4 thin films," *Thin Solid Films*, vol. 517, no. 7, pp. 2524–2526, 2009.

[16] T. Tanaka, D. Kawasaki, M. Nishio, Q. Guo, and H. Ogawa, "Fabrication of Cu_2ZnSnS_4 thin films by co-evaporation," *Physica Status Solidi C*, vol. 3, no. 8, pp. 2844–2847, 2006.

[17] P. A. Cormier and R. Snyders, "One-step synthesis of Cu_2ZnSnS_4 thin films by reactive magnetron co-sputtering," *Acta Materialia*, vol. 96, pp. 80–88, 2015.

[18] C. P. Chan, H. Lam, and C. Surya, "Preparation of Cu_2ZnSnS_4 films by electrodeposition using ionic liquids," *Solar Energy Materials and Solar Cells*, vol. 94, no. 2, pp. 207–211, 2010.

[19] J. J. Scragg, P. J. Dale, and L. M. Peter, "Synthesis and characterization of Cu_2ZnSnS_4 absorber layers by an electrodeposition-annealing route," *Thin Solid Films*, vol. 517, no. 7, pp. 2481–2484, 2009.

[20] Y. B. K. Kumar, P. U. Bhaskar, G. S. Babu, and V. S. Raja, "Effect of copper salt and thiourea concentrations on the formation of Cu_2ZnSnS_4 thin films by spray pyrolysis," *Physica Status Solidi A: Applications and Materials Science*, vol. 207, no. 1, pp. 149–156, 2010.

[21] J. Iljina, R. Zhang, M. Ganchev et al., "Formation of Cu_2ZnSnS_4 absorber layers for solar cells by electrodeposition–annealing route," *Thin Solid Films*, vol. 537, pp. 85–89, 2013.

[22] J. He, L. Sun, N. Ding et al., "Single-step preparation and characterization of $Cu_2ZnSn(S_xSe_{1-x})_4$ thin films deposited by pulsed laser deposition method," *Journal of Alloys and Compounds*, vol. 529, pp. 34–37, 2012.

[23] K. Moriya, K. Tanaka, and H. Uchiki, "Cu_2ZnSnS_4 thin films annealed in H_2S atmosphere for solar cell absorber prepared by pulsed laser deposition," *Japanese Journal of Applied Physics*, vol. 47, no. 1, pp. 602–604, 2008.

[24] L. Sun, J. He, H. Kong, F. Yue, P. Yang, and J. Chu, "Structure, composition and optical properties of Cu_2ZnSnS_4 thin films deposited by pulsed laser deposition method," *Solar Energy Materials and Solar Cells*, vol. 95, no. 10, pp. 2907–2913, 2011.

[25] P. Spinelli, F. Lenzmann, A. Weeber, and A. Polman, "Effect of EVA encapsulation on antireflection properties of mie nanoscatterers for c-Si solar cells," *IEEE Journal of Photovoltaics*, vol. 5, pp. 559–564, 2015.

[26] O. Breitenstein, "An alternative one-diode model for illuminated solar cells," *IEEE Journal of Photovoltaics*, vol. 4, no. 3, pp. 899–905, 2014.

[27] K. Oishi, G. Saito, K. Ebina et al., "Growth of Cu_2ZnSnS_4 thin films on Si (100) substrates by multisource evaporation," *Thin Solid Films*, vol. 517, no. 4, pp. 1449–1452, 2008.

[28] T. K. Todorov, K. B. Reuter, and D. B. Mitzi, "High-efficiency solar cell with earth-abundant liquid-processed absorber," *Advanced Materials*, vol. 22, no. 20, pp. E156–E159, 2010.

[29] C. Shao, H. Guan, Y. Liu, and R. Mu, "MgO nanofibres via an electrospinning technique," *Journal of Materials Science*, vol. 41, no. 12, pp. 3821–3824, 2006.

[30] O. Toprakci, L. Ji, Z. Lin, H. A. K. Toprakci, and X. Zhang, "Fabrication and electrochemical characteristics of electrospun $LiFePO_4$/carbon composite fibers for lithium-ion batteries," *Journal of Power Sources*, vol. 196, no. 18, pp. 7692–7699, 2011.

[31] M. Jeon, T. Shimizu, and S. Shingubara, "Cu_2ZnSnS_4 thin films and nanowires prepared by different single-step electrodeposition method in quaternary electrolyte," *Materials Letters*, vol. 65, no. 15-16, pp. 2364–2367, 2011.

[32] K.-C. Hsu, J.-D. Liao, J.-R. Yang, and Y.-S. Fu, "Cellulose acetate assisted synthesis and characterization of kesterite quaternary semiconductor Cu_2ZnSnS_4 mesoporous fibers by an electrospinning process," *CrystEngComm*, vol. 15, no. 21, pp. 4303–4308, 2013.

[33] A. Singh, H. Geaney, F. Laffir, and K. M. Ryan, "Colloidal synthesis of wurtzite Cu_2ZnSnS_4 nanorods and their perpendicular assembly," *Journal of the American Chemical Society*, vol. 134, no. 6, pp. 2910–2913, 2012.

[34] A. S. Ibraheam, Y. Al-Douri, U. Hashim et al., "Cadmium effect on optical properties of $Cu_2Zn_{1-x}Cd_xSnS_4$ quinternary alloys nanostructures," *Solar Energy*, vol. 114, pp. 39–50, 2015.

[35] Y. Al-Douri, Q. Khasawneh, S. Kiwan et al., "Structural and optical insights to enhance solar cell performance of CdS nanostructures," *Energy Conversion and Management*, vol. 82, pp. 238–243, 2014.

[36] Y. Al-Douri, H. Abid, and H. Aourag, "Correlation between the bulk modulus and the charge density in semiconductors," *Physica B*, vol. 305, no. 2, pp. 186–190, 2001.

[37] A. M. Sherry and M. Kumar, "Analysis of thermal expansion for alkali halide crystals using the isobaric equation of state," *Journal of Physics and Chemistry of Solids*, vol. 52, no. 9, pp. 1145–1148, 1991.

[38] J. L. Tallon, "The thermodynamics of elastic deformation-I: equation of state for solids," *Journal of Physics and Chemistry of Solids*, vol. 41, no. 8, pp. 837–850, 1980.

[39] J. Barman, K. C. Sarma, M. Sarma, and K. Sarma, "Structural and optical studies of chemically prepared CdS nanocrystalline thin films," *Indian Journal of Pure and Applied Physics*, vol. 46, no. 5, pp. 339–343, 2008.

[40] M. A. Mahdi, S. J. Kasem, J. J. Hassen, A. A. Swadi, and S. K. J. A. l-Ani, "Structural and optical properties of Chemical deposition CdS thin films," *International Journal Nanoelectronics & Materials*, vol. 2, pp. 163–172, 2009.

[41] R. Sahraei, S. Shahriyar, M. H. Majles Ara, A. Daneshfar, and N. Shokri, "Preparation of nanocrystalline CdS thin films by a new chemical bath deposition route for application in solar cells as antireflection coatings," *Progress in Color Colorants and Coating*, vol. 3, pp. 82–90, 2010.

[42] J. C. Phillips, *Bands and Bonds in Semiconductors*, Academic Press, San Diego, Calif, USA, 1973.

[43] W. A. Harison, *Electronic Structure and Properties of Solids*, General Publishing Company, Toronto, Canada, 1989.

[44] M. L. Cohen, "Calculation of bulk moduli of diamond and zinc-blende solids," *Physical Review B*, vol. 32, no. 12, pp. 7988–7991, 1985.

[45] P. K. Lam, M. L. Cohen, and G. Martinez, "Analytic relation between bulk moduli and lattice constants," *Physical Review B*, vol. 35, no. 17, pp. 9190–9194, 1987.

[46] Y. Al-Douri, H. Abid, and H. Aourag, "Empirical formula relating the bulk modulus to the lattice constant in tetrahedral semiconductors," *Materials Chemistry and Physics*, vol. 87, no. 1, pp. 14–17, 2004.

[47] L.-J. Chen and Y.-J. Chuang, "Directly electrospinning growth of single crystal Cu_2ZnSnS_4 nanowires film for high performance thin film solar cell," *Journal of Power Sources*, vol. 241, pp. 259–265, 2013.

[48] K. H. Lee, H. Y. Kim, H. J. Bang, Y. H. Jung, and S. G. Lee, "The change of bead morphology formed on electrospun polystyrene fibers," *Polymer*, vol. 44, no. 14, pp. 4029–4034, 2003.

[49] P. A. Luque, M. A. Quevedo-Lopez, and A. Olivas, "Influence of deposition time on ZnS thin film growth over SiO_2 and glass substrates," *Materials Letters*, vol. 106, pp. 49–51, 2013.

[50] N. M. Balzaretti and J. A. H. Da Jornada, "Pressure dependence of the refractive index of diamond, cubic silicon carbide and cubic boron nitride," *Solid State Communications*, vol. 99, no. 12, pp. 943–948, 1996.

[51] N. M. Ravindra, S. Auluck, and V. K. Srivastava, "On the penn gap in semiconductors," *Physica Status Solidi B*, vol. 93, no. 2, pp. K155–K160, 1979.

[52] P. J. L. Hervé and L. K. J. Vandamme, "Empirical temperature dependence of the refractive index of semiconductors," *Journal of Applied Physics*, vol. 77, no. 10, pp. 5476–5477, 1995.

[53] D. K. Ghosh, L. K. Samanta, and G. C. Bhar, "A simple model for evaluation of refractive indices of some binary and ternary mixed crystals," *Infrared Physics*, vol. 24, no. 1, pp. 43–47, 1984.

[54] Y. Al-Douri, H. Khachai, and R. Khenata, "Chalcogenides-based quantum dots: optical investigation using first-principles calculations," *Materials Science in Semiconductor Processing*, vol. 39, pp. 276–282, 2015.

[55] Y. Al-Douri, U. Hashim, R. Khenata et al., "Ab initio method of optical investigations of $CdS_{1-x}Te_x$ alloys under quantum dots diameter effect," *Solar Energy*, vol. 115, pp. 33–39, 2015.

[56] T. S. Moss, "A relationship between the refractive index and the infra-red threshold of sensitivity for photoconductors," *Proceedings to the Physical Society: Section B*, vol. 63, no. 3, article no. 302, pp. 167–176, 1950.

[57] V. P. Gupta and N. M. Ravindra, "Comments on the moss formula," *Physica Status Solidi (B)*, vol. 100, no. 2, pp. 715–719, 1980.

[58] P. Herve and L. K. J. Vandamme, "General relation between refractive index and energy GAP in semiconductors," *Infrared Physics & Technology*, vol. 35, no. 4, pp. 609–615, 1994.

[59] D. R. Penn, "Wave-number-dependent dielectric function of semiconductors," *Physical Review*, vol. 128, no. 5, pp. 2093–2097, 1962.

[60] J. A. Van Vechten, "Quantum dielectric theory of electronegativity in covalent systems. I. Electronic dielectric constant," *Physical Review*, vol. 182, no. 3, pp. 891–905, 1969.

[61] G. A. Samara, "Temperature and pressure dependences of the dielectric constants of semiconductors," *Physical Review B*, vol. 27, no. 6, pp. 3494–3505, 1983.